

The stellar mass function, binary content and radial structure of the open cluster Praesepe derived from PPMXL and SDSS data

P. Khalaj* and H. Baumgardt

School of Mathematics and Physics, University of Queensland, St. Lucia, QLD 4072, Australia

Accepted 2013 July 05. Received 2013 July 05; in original form 2013 February 24

ABSTRACT

We have determined possible cluster members of the nearby open cluster Praesepe (M44) based on J and K photometry and proper motions from the PPMXL catalogue and z photometry from the Sloan Digital Sky Survey (SDSS). In total we identified 893 possible cluster members down to a magnitude of $J = 15.5$ mag, corresponding to a mass of about $0.15 M_{\odot}$ for an assumed cluster distance modulus of $(m - M)_0 = 6.30$ mag ($d \approx 182$ pc), within a radius of 3.5° around the cluster centre. We derive a new cluster centre for Praesepe ($\alpha_{\text{centre}} = 8^{\text{h}}39^{\text{m}}37^{\text{s}}$, $\delta_{\text{centre}} = 19^{\circ}35'02''$). We also derive a total cluster mass of about $630 M_{\odot}$ and a 2D half-number and half-mass radius of 4.25 pc and 3.90 pc respectively. The global mass function (MF) of the cluster members shows evidence for a turnover around $m = 0.65 M_{\odot}$. While more massive stars can be fit by a power-law $\xi(m) \sim m^{-\alpha}$ with slope $\alpha = 2.88 \pm 0.22$, stars less massive than $m = 0.65 M_{\odot}$ are best fitted with $\alpha = 0.85 \pm 0.10$. In agreement with its large dynamical age, we find that Praesepe is strongly mass segregated and that the mass function slope for high mass stars steepens from a value of $\alpha = 2.32 \pm 0.24$ inside the half-mass radius to $\alpha = 4.90 \pm 0.51$ outside the half-mass radius. We finally identify a significant population of binaries and triples in the colour-magnitude diagram of Praesepe. Assuming non-random pairing of the binary components, a binary fraction of about 35% for primaries in the mass range $0.6 < m/M_{\odot} < 2.20$ is required to explain the observed number of binaries in the colour-magnitude diagram (CMD).

Key words: stars: mass function — open clusters and associations: individual: Praesepe

1 INTRODUCTION

Open clusters are important test beds for star formation, stellar initial mass function (IMF) and stellar evolution theories (Gaburov & Gieles 2008), since they provide statistically significant samples of stars of known distance, age and metallicity. The identification of cluster members is especially easy in nearby clusters ($d < 200$ pc) since these have on average large proper motions which allow to effectively separate cluster members from background stars. With a distance modulus of $(m - M)_0 = 6.30 \pm 0.07$ mag (van Leeuwen 2009) ($d = 181.97^{+5.96}_{-5.77}$ pc) Praesepe is one of the nearest clusters to the Sun. Due to its proximity, Praesepe has been studied extensively in the past. However, so far no consensus on the stellar distribution and low-mass mass function has been reached. Proper motion studies of the bright members were first carried out by Klein-Wassink (1927), Jones

& Cudworth (1983) and Jones & Stauffer (1991), who determined members down to $V \sim 18$ mag, corresponding to masses of about $0.3 M_{\odot}$. Hambly et al. (1995) presented cluster members down to $0.1 M_{\odot}$ in the central 19 deg^2 using images taken by the United Kingdom Schmidt Telescope (UKST). They found evidence for mass segregation in Praesepe and a rising mass function from $1 M_{\odot}$ down to $0.1 M_{\odot}$, the limit of their survey. Pinfield et al. (1997) conducted a photometric survey of Praesepe in RIZ -bands down to $I = 21.5$ using the Isaac Newton Telescope (INT). They also found a rising mass function ($\xi(m) \sim dN/dm \sim m^{-\alpha}$) from $0.15 M_{\odot}$ down to $0.07 M_{\odot}$ with slope $\alpha \geq 1.5$. In contrast, using proper motions derived from the Two Micron All Sky Survey (2MASS) and the Palomar Observatory Sky Survey, Adams et al. (2002) found that the low-mass stellar mass function below $0.4 M_{\odot}$ can be fitted by a flat mass function with $\alpha \approx 0$ and only a marginal radial dependence of the mass function. Chappelle et al. (2005) probed the central 2.6 deg^2 of Praesepe using I -band data down to $I \sim 21.3$ mag

* E-mail: pouria.khalaj@uqconnect.edu.au

and Z -band data down to $Z \sim 20.5$ mag, from images taken by the INT/ Wide Field Camera (WFC) and near-infrared follow-up measurements using the United Kingdom Infrared Telescope (UKIRT) Fast Track Imager (UFTI). They found a rising mass function from $1 M_{\odot}$ down to $0.1 M_{\odot}$. [González-García et al. \(2006\)](#) conducted deep photometric searches for sub-stellar members of Praesepe using the Sloan i' and z' broad-band filters, with the 3.5-meter and the 5-meter Hale telescopes on the Calar Alto and Palomar Observatories. The total area that they surveyed was 1177 arcmin^2 and the 5σ detection limit of their survey was $i' = 24.5$ mag and $z' = 24$ mag, which corresponds to $m = 50 - 55 M_{\text{Jup}}$. They found that the mass function of Praesepe strongly depends on the adopted cluster age and at the youngest possible ages of Praesepe (500-700 Myr), their analysis suggests a rapidly decreasing mass function for brown dwarfs. [Kraus & Hillenbrand \(2007\)](#) combined archival survey data from SDSS, 2MASS, USNO-B1.0 and UCAC-2.0 and found 1010 stars in Praesepe as candidate members with probability $p > 80\%$. Their result for the mass function of Praesepe is similar to that of [Hambly et al. \(1995\)](#), i.e a rise from $1 M_{\odot}$ down to $0.1 M_{\odot}$. [Boudreault et al. \(2010\)](#) performed an optical (I_c -band) and near-infrared (J and K_s -band) photometric survey of the innermost 3.1 deg^2 of Praesepe with 5σ detection limits of $I_c = 23.4$ mag and $J = 20.0$ mag. They observed that the mass function of Praesepe rises from $0.6 M_{\odot}$ down to $0.1 M_{\odot}$ with $\alpha = 1.8 \pm 0.1$ and turns over at $\sim 0.1 M_{\odot}$. [Baker et al. \(2010\)](#) found a moderately rising mass function with $\alpha = 1.11 \pm 0.37$ for the mass range $0.6 M_{\odot}$ to $0.125 M_{\odot}$ in the UKIRT Infrared Deep Sky Survey Galactic Clusters Survey (UKIDSS GCS) for $Z < 18$. Using observations from the Large Binocular Telescope (LBT) in the $rizY$ bands, [Wang et al. \(2011\)](#) identified 62 cluster member candidates (40 of which are sub-stellar) within the central 0.59 deg^2 of Praesepe down to a 5σ detection limit of $i \sim 25.6$ mag ($\sim 40 M_{\text{Jup}}$). They found that the mass function of Praesepe shows a rise from $105 M_{\text{Jup}}$ to $60 M_{\text{Jup}}$ and then a turnover at $\sim 60 M_{\text{Jup}}$. More recently, [Boudreault et al. \(2012\)](#) found 1116 cluster candidates in a $\sim 36 \text{ deg}^2$ field based on a 3σ astrometric and five-band ($ZYJHK$) photometric selection, using the Data Release 9 (DR9) of UKIDSS GCS. They found that the mass function of Praesepe has a maximum at $\sim 0.6 M_{\odot}$ and then decreases to the lowest mass bin of $0.056 M_{\odot}$.

In the present paper, we determine Praesepe members based on the PPMXL catalogue ([Röser et al. 2010](#)) and SDSS DR9. Our paper is structured as follows: we first discuss the observational data in section 2. In section 3 we discuss the procedures we have followed to determine possible members. Our results are presented in section 4 and we finally summarize our work in section 5.

2 OBSERVATIONAL DATA

In this study we combine data from the PPMXL catalogue ([Röser et al. 2010](#)) with z magnitudes from SDSS DR9 ([Ahn et al. 2012](#)). PPMXL catalogue combines the USNO-B1.0 ([Monet et al. 2003](#)) and 2MASS catalogues ([Skrutskie et al. 2006](#)) yielding the largest collection of proper motions in the International Celestial Reference Frame (ICRS) to date ([Röser et al. 2010](#)). USNO-B1.0 contains the positions of

more than one billion objects taken photographically around 1960; 2MASS is an all-sky survey conducted in the years 1997 to 2001 in the J , H and K_s bands. In PPMXL, data from USNO-B1.0 are used as the first epoch images and those from 2MASS as the second epoch images, deriving the mean positions and proper motions for 910,468,710 objects from the brightest magnitudes down to $V \approx 20$ mag ([Röser et al. 2010](#)). Mean errors of the proper motions vary from ~ 4 milli-arcseconds per year (mas/yr) for $J < 10$ mag to more than 10 mas/yr at $J > 16$ mag.

The field of Praesepe is also covered in the SDSS DR9. A cross-matching between SDSS and PPMXL shows that SDSS is $\sim 95\%$ complete within 5 deg from the centre of Praesepe for stars with $J \leq 15.5$ mag but does not contain stars beyond 5.5° from the centre of Praesepe. SDSS data covers five optical bands ($ugriz$) to a depth of $g \sim 23$ mag ([York et al. 2000](#)).

3 MEMBERSHIP DETERMINATION

3.1 Astrometric membership

We restrict our study to a radius of 3.5 degrees from the centre of Praesepe ($\alpha = 8^h 40^m 00^s$, $\delta = 19^\circ 30' 00''$ [Lyngå 1987](#)). The reason of this choice is that the tidal radius of Praesepe is $r_t = 3.5^\circ \pm 0.1^\circ$ ([Kraus & Hillenbrand 2007](#)) suggesting that stars beyond this point are more likely to be background stars. We present our estimation of the background contamination within this radius in section 3.4.

Within the search area, cluster members are selected based on proper motions followed by two photometric tests, both of which are described in more detail further below. We restrict ourselves to stars with $J < 15.5$ mag whose proper motion errors are about ~ 4 mas/yr. For fainter stars the proper motion errors become much larger than 10 mas/yr. A comparison of PPMXL with [Boudreault et al. \(2012\)](#) shows that PPMXL is about 93% complete down to $J = 15.5$ mag, but becomes incomplete for fainter magnitudes.

We first select cluster members based on their proper motions. We use a χ^2 test to separate cluster members from field stars, i.e. for each star i , we calculate a χ^2 value according to:

$$\chi_i^2 = \frac{(\mu_{\alpha i} - \bar{\mu}_{\alpha})^2}{e_{\alpha i}^2 + e_{\alpha}^2 + \sigma_{\alpha}^2} + \frac{(\mu_{\delta i} - \bar{\mu}_{\delta})^2}{e_{\delta i}^2 + e_{\delta}^2 + \sigma_{\delta}^2} < 6.17 \quad (1)$$

where $\mu_{\alpha i}$ and $\bar{\mu}_{\alpha}$ are the proper motion of star i and the average cluster proper motion in right ascension, $\mu_{\delta i}$ and $\bar{\mu}_{\delta}$ are the proper motion of star i and the average cluster proper motion in declination, $e_{\alpha i}$, e_{α} , $e_{\delta i}$, e_{δ} are the corresponding errors and σ_{α} and σ_{δ} are the components of the internal velocity dispersion. For the mean cluster motion and the corresponding errors we use $\bar{\mu}_{\alpha} = -35.81$ mas/yr, $\bar{\mu}_{\delta} = -12.85$ mas/yr, $e_{\alpha} = 0.29$ mas/yr and $e_{\delta} = 0.24$ mas/yr as determined by [van Leeuwen \(2009\)](#). We also assume a one-dimensional internal velocity dispersion of $\sigma_v = 0.67 \pm 0.23$ km/sec ([Madsen et al. 2002](#)), which corresponds to a proper motion of $\sigma_v = 0.78$ mas/yr at the distance of Praesepe. As the threshold separating members from non-members we assume $\chi^2 = 6.17$, equivalent to a 95.4% (1.5 sigma) limit for two independent degrees of freedom. Table 1 summarizes the parameters for Praesepe.

Table 1. Praesepe parameters. (α_0, δ_0) : cluster centre (see Sec. 3.3); (μ_α, μ_δ) : mean proper motion of the cluster; (e_α, e_δ) : proper motion mean error; σ_v : one-dimensional internal velocity dispersion

parameter	value	reference
α_0	$08^h39^m37^s$	Our work, 2013
δ_0	$+19^\circ35'02''$	
$(m - M)_0$	6.30 ± 0.07 mag	van Leeuwen (2009)
μ_α	-35.81 mas/yr	
e_α	0.29 mas/yr	
μ_δ	-12.85 mas/yr	
e_δ	0.24 mas/yr	
σ_v	0.67 ± 0.23 km/sec	Madsen et al. (2002)
$\log(\text{age})$	8.77 ± 0.1 dex	Fossati et al. (2008)
$E(B - V)$	0.027 ± 0.004 mag	Taylor (2006)
[Fe/H]	0.11 ± 0.03 dex	An et al. (2007)

We ignore stars with very large proper motion errors ($e_\alpha > 15$ mas/yr) in PPMXL since a separation into field and cluster stars is not possible for them given the absolute value of the proper motion of Praesepe (see also Fig. 1). We ignore projection effects due to the different location of stars on the sky since they amount to only 0.07 mas/yr difference in proper motion, significantly smaller than the error bars in PPMXL. We also ignore distance effects due to the different radial distances of stars along the light of sight. This distance effect only adds an uncertainty of about 2 mas/yr which is small compared to the typical proper motion error of PPMXL, although it could be important for bright stars.

Figure 1 shows the proper motions of all PPMXL stars in a field of 3.5° in radius. Stars that pass our kinematic test are shown in red. From 45870 stars with $J \leq 15.5$ mag and $e_\alpha, e_\delta \leq 10$ mas/yr that reside within 3.5° from the cluster centre, 1613 stars meet our χ^2 criterion.

3.2 Photometric membership

We use the latest version of the PADOVA stellar evolution models¹ from Marigo et al. (2008) and Girardi et al. (2010) to estimate the colours and magnitudes of the cluster members based on their metallicity, age and extinction. We use the J and K_s bands of the PADOVA models to create an isochrone. In addition to PADOVA isochrones, we also use two more isochrones from Hauschildt et al. (1999) (NextGen models) and Allard et al. (2011) (BT-Settl models) for comparison. In our study, we adopt an age of 590 Myrs (Fossati et al. 2008), an extinction of $E(B - V) = 0.027$ mag (Taylor 2006) and a distance modulus of $(m - M)_0 = 6.30 \pm 0.07$ mag (van Leeuwen 2009) for Praesepe. A number of values have been found for the metallicity of Praesepe: $+0.13 \pm 0.007$ dex (Boesgaard & Budge 1988); $+0.125 \pm 0.032$ dex (Boesgaard 1989); $[\text{Fe}/\text{H}] = +0.038 \pm 0.039$ dex (Friel & Boesgaard 1992); 0.11 ± 0.03 dex from spectroscopy and $+0.20 \pm 0.04$ dex from photometry (An et al. 2007) and $+0.27 \pm 0.10$ dex (Pace

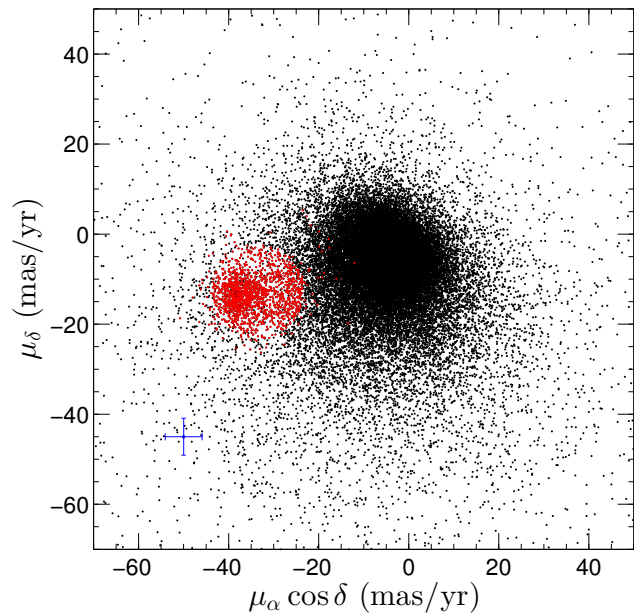


Figure 1. Plot of the proper motions of all PPMXL stars in a field of 3.5° from the centre of Praesepe (black dots) and the stars that satisfy the proper motion test described by Eq. (1) (red dots). The mode of the proper motion errors is shown by the blue cross in the lower left corner.

et al. 2008). Since the location of stars in the CMD is not very sensitive to the adopted metallicity, we only consider $[\text{Fe}/\text{H}] = 0.11 \pm 0.03$ dex (An et al. 2007).

Fig. 2 shows the distribution of the stars that pass the kinematic test in a CMD as well as the corresponding PADOVA ($T = 590$ Myr, $[\text{Fe}/\text{H}] = 0.11$ dex), NextGen and BT-Settl (both with $T = 590$ Myr, $[\text{Fe}/\text{H}] = 0$ dex) isochrones for comparison. We require that photometric members lie within 2.5σ of the isochrones in the J vs $J - K_s$ colour magnitude diagram where σ refers to the mean error of photometry for each star. It can be seen from Fig. 2 that the proper motion selected stars agree reasonably well with the PADOVA isochrone down to $J = 11.75$ mag, which corresponds to about $0.7 M_\odot$. However, starting from $J = 11.75$ mag, the PADOVA isochrone disagrees with the actual location of the possible Praesepe members in the CMD as the isochrone predicts faint (low-mass) stars to be bluer than observed. Since this disagreement is virtually insensitive to the assumed age, metallicity and distance modulus, we reason that this is due to the inherent limitations in the PADOVA isochrone for low-mass stars. Similar results have been obtained by Röser et al. (2011) for the Hyades.

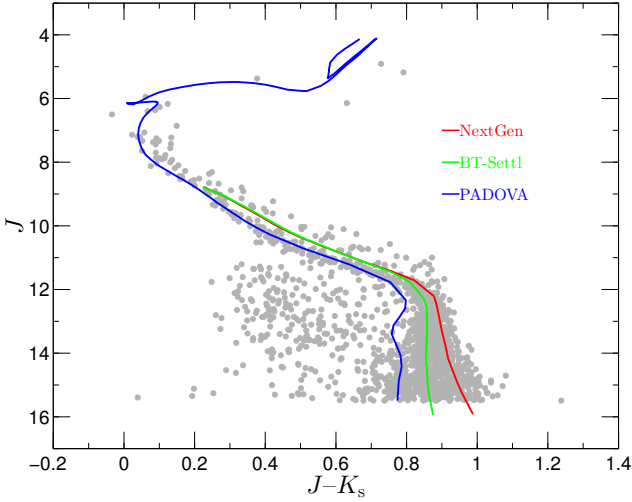
In order to select faint cluster members photometrically, we shift the PADOVA isochrone by $+0.1$ mag for magnitudes fainter than $J = 11.75$ mag. This seems better than using the BT-Settl or NextGen isochrones since these isochrones are still a bit off at faint magnitudes and they are off at bright magnitudes as well.

Fig. 3 depicts the stars that satisfy both the proper motion and photometric requirements (filled red circles). The blue line is the modified isochrone which determines the photometric membership of the PM-selected members and it matches the average location of the cluster members very well. The green-filled triangles and open magenta squares

¹ <http://stev.oapd.inaf.it/cgi-bin/cmd>

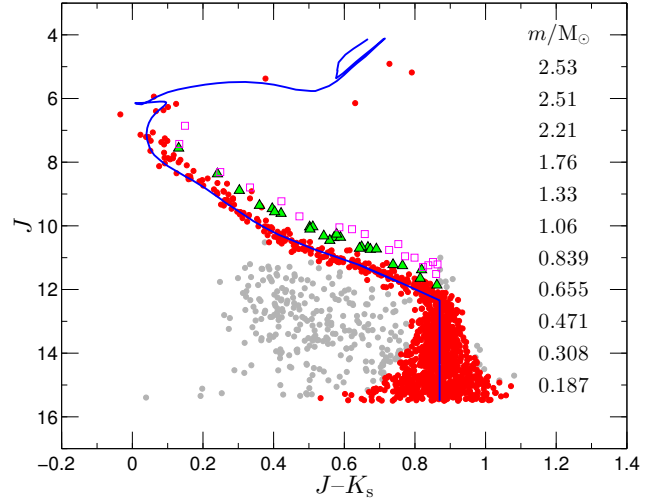
Table 2. Celestial coordinates, proper motions, magnitudes and the masses of the possible members of Praesepe sorted by right ascension. Table 2 is available in its entirety in the electronic version of the journal.

RA (J2000) (deg)	Dec. (J2000) (deg)	$\mu_\alpha \cos \delta$ (mas/yr)	μ_δ (mas/yr)	J (mag)	K_s (mag)	Mass (M_\odot)
126.423399	+19.511820	-33.0 ± 4.2	-14.0 ± 4.2	15.066 ± 0.039	14.168 ± 0.048	0.183
126.572703	+19.726598	-36.2 ± 4.2	-13.7 ± 4.2	13.896 ± 0.025	12.981 ± 0.024	0.327
126.597027	+19.551072	-35.6 ± 4.2	-22.8 ± 4.2	14.643 ± 0.032	13.696 ± 0.034	0.225
...
133.536124	+18.477437	-27.1 ± 3.7	-08.6 ± 3.7	11.910 ± 0.023	11.081 ± 0.020	0.675
133.541163	+19.946329	-26.6 ± 3.7	-12.8 ± 3.7	12.233 ± 0.020	11.385 ± 0.021	0.618
133.580451	+19.718509	-36.0 ± 3.7	-21.4 ± 3.7	11.090 ± 0.022	10.452 ± 0.018	0.825

**Figure 2.** Colour-magnitude diagram of the stars selected by proper motions (filled grey circles). Solid blue, green and red lines show the PADOVA (left), BT-Settl (middle) and NextGen (right) isochrones respectively.

show the possible binary and multiple stars which are discussed in section 4.3.

There are 1286 stars that satisfy both tests, however, due to the relatively large errors of proper motion and photometry of faint stars we expect a significant contamination of field stars for magnitudes $J > 12$ mag. In order to remove possible contaminants with $J > 12$ mag we apply a second photometric test using z magnitudes from SDSS and K_s magnitudes from 2MASS. Fig. 4 shows the position of all stars with $J > 12$ mag in a z versus $z - K_s$ diagram. One can see that in this CMD, the NextGen isochrone matches the actual position of possible members. As a result we use this isochrone to remove background stars photometrically. We require that each photometric member lies within 2.5σ of the isochrone (filled red circles) or its color index differs by no more than $-0.1/+0.25$ mag from the corresponding color index of the isochrone at the same magnitude (filled magenta circles). This additional condition is added since we observe that there are a number of stars (enclosed by the dashed blue lines in Fig. 4), which are not identified as photometric members due to their small photometric errors but are concentrated towards the cluster centre and have a χ^2 distribution clustered around zero. As a result we keep these stars as photometric members. In contrast, the stars

**Figure 3.** Colour-magnitude diagram of the stars selected by proper motion and photometry. Filled red circles show stars that satisfy both tests (1286 stars). The filled grey circles show stars that do not pass the photometric test. Inspection of the spatial position of these stars shows that they are evenly spread across the survey region and the distribution of their χ^2 values shows no clustering around zero, hence these stars are most likely field stars. The green-filled triangles show possible binaries (25 stars) and open magenta squares show possible multiples (18 stars). The blue line denotes the modified PADOVA isochrone.

shown as filled grey circles in Fig. 4 have a flat χ^2 distribution and are uniformly spread in our 3.5-degree survey field. We end up with 893 stars which satisfy the astrometric and all photometric tests. Figure 5 shows the spatial distribution of these stars. We also obtain the mass of the possible members by interpolating the theoretical masses from the PADOVA isochrone using the J magnitudes. These masses are listed in Table 2.

3.3 Cluster centre

Before obtaining surface density plots, we first determine a new coordinate for the cluster centre (density centre). The density centre as defined by von Hoerner (1960, 1963) is the density weighted average of the positions of all stars:

$$\vec{r}_{d,j} \equiv \frac{\sum_i \vec{r}_i \rho_j^{(i)}}{\sum_i \rho_j^{(i)}} \quad (2)$$

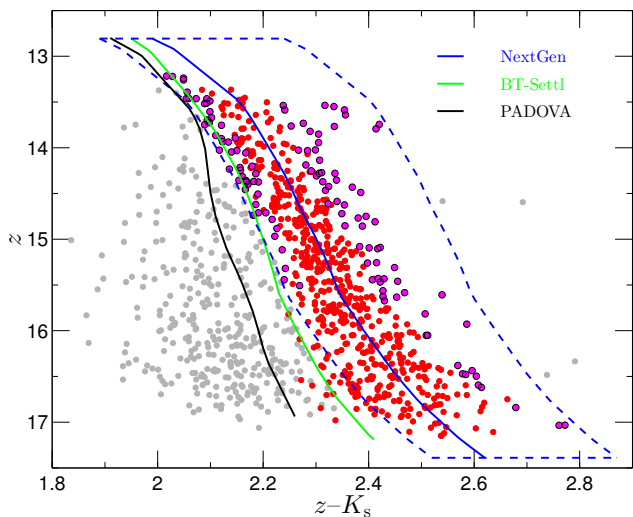


Figure 4. Colour-magnitude diagram of all stars with $J > 12$ which are selected by the first photometric test (1020 stars). Filled red circles show stars lie within 2.5σ of the isochrone (528 stars). The filled magenta circles show those stars which are designated as candidate members due to their spatial position and χ^2 distribution of proper motions (124 stars). The filled grey circles show the stars that fail the second photometric test, hence they are assumed as non-members (368 stars). PADOVA (left), BT-Settl (middle) and NextGen (right) isochrones are represented by black, green and solid blue lines respectively.

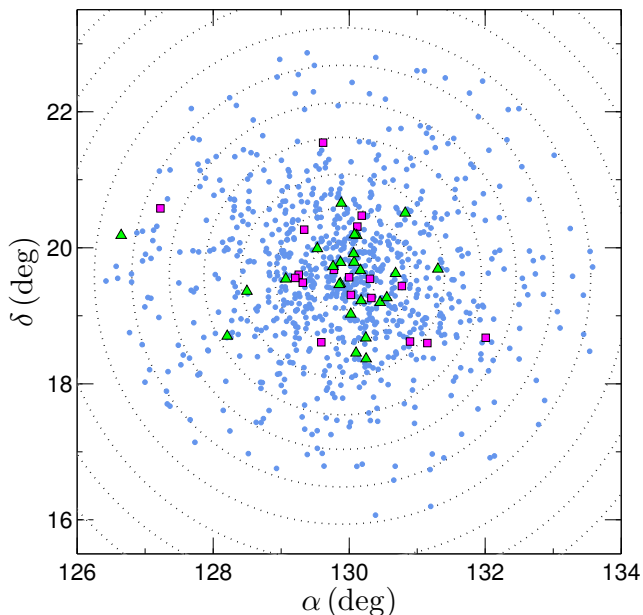


Figure 5. Spatial distribution of the possible cluster members of Praesepe (893 stars) with respect to the new centre of Praesepe. The filled green triangles and the filled magenta squares show possible binaries and multiples. Dotted grey circles are spaced by 0.5° .

where $\rho_j^{(i)}$ is the local density estimator of order j around the i th particle with position vector \vec{r}_i . We replace the 3D density estimator $\rho_j^{(i)}$ by the surface density $\Sigma_j^{(i)}$. To estimate $\vec{r}_{d,j}$ we adopt the unbiased form of the density estimator introduced by Casertano & Hut (1985) and consider the 10 nearest neighbours of each star to obtain $\Sigma_j^{(i)}$. We then obtain the new coordinate of the cluster centre as follows:

$$\alpha_{\text{centre}} = 8^{\text{h}}39^{\text{m}}37^{\text{s}} \quad \delta_{\text{centre}} = 19^\circ35'02''$$

This new centre differs by about $5''$ from the coordinate of the cluster center given by Lyngå (1987) ($\alpha_{\text{centre}} = 8^{\text{h}}40^{\text{m}}00^{\text{s}}$, $\delta_{\text{centre}} = 19^\circ30'00''$).

3.4 Surface density profile

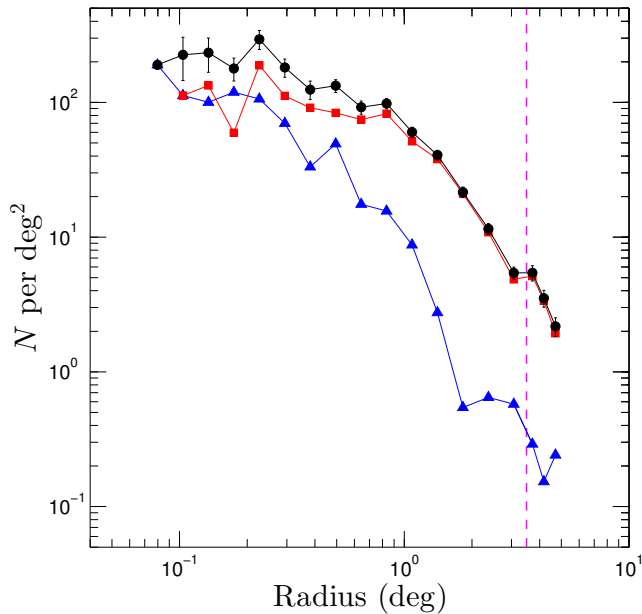
To determine the distribution of member stars and the possible background stars, we first consider a field of 5° and divide this field into 18 radial bins from 0° to 5° where SDSS is $\sim 95\%$ complete.

We then consider all stars that satisfy the astrometric and photometric selection criteria in this field and plot the surface density of faint ($11 < J \leq 15.5$), bright ($J \leq 11$) and all stars ($J \leq 15.5$) in each bin as a function of radius from the new centre of Praesepe in Fig. 6. At the distance of Praesepe $J = 11$ mag corresponds to $m = 0.84 M_\odot$. Error bars only consider the statistical uncertainties in the number of stars. One can see that the density profiles do not level off beyond the tidal radius of Praesepe. This is in agreement with Küpper et al. (2010) who showed that the surface density profiles of star clusters extend beyond the tidal radius due to stars escaping the cluster. To estimate an upper limit for the density of background stars, we therefore consider the density of the last radial bin and find that the background density of stars is 2.17 ± 0.34 stars/deg², implying that there are still about 84 background stars within a field of 3.5 degrees from the centre of Praesepe. Since we found 893 candidate stars in total within the same area, the background contamination is $\sim 10\%$ and needs to be considered when determining the mass function of cluster members and the total cluster mass. We will statistically subtract these background stars when deriving the mass function. The details of this subtraction are explained in Sec. 4.1.

Fig. 7 shows the cumulative sums of stellar masses for faint, bright and all stars as a function of radius in the search field of 3.5° . The two-dimensional half-number radius and half-mass radius are 1.34° and 1.23° which correspond to 4.25 pc and 3.90 pc respectively. Assuming that the corresponding 3D radii are 1/3 larger than the projected radii, we find that the 3D half-number and half-mass radii are 5.67 and 5.20 pc respectively. Table 3 summarizes half-mass and half-number radii corresponding to faint, bright and all stars. The fact that the 2D half-mass and half-number radii of all cluster stars are about 2 times larger than those of bright stars evidently shows that Praesepe is strongly mass segregated. Mass segregation of Praesepe can also be inferred from Fig. 8 which shows the average mass of the possible cluster members as a function of radius from the new cluster centre. One can see that the average mass of stars is $0.96 \pm 0.08 M_\odot$ inside 0.3 pc and drops down to $\sim 0.45 M_\odot$ outside the half-mass radius.

Table 3. Table of projected half-number and half-mass radii for cluster members

type of stars	number of stars	half-number radius (2D)	half-mass radius (2D)
Faint Stars $11 < J \leq 15.5$	759 stars	1.23° 3.90 pc	1.34° 4.25 pc
Bright Stars $J \leq 11$	134 stars	0.65° 2.07 pc	0.64° 2.04 pc
All Stars $J \leq 15.5$	893 stars	1.34° 4.25 pc	1.23° 3.90 pc

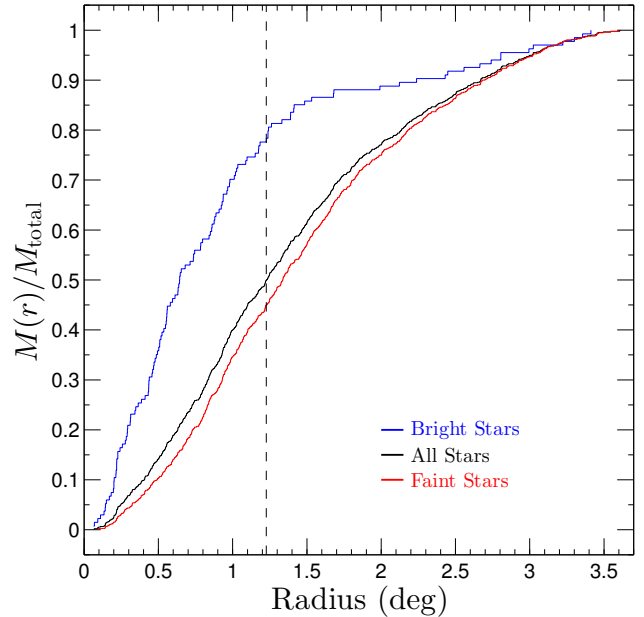
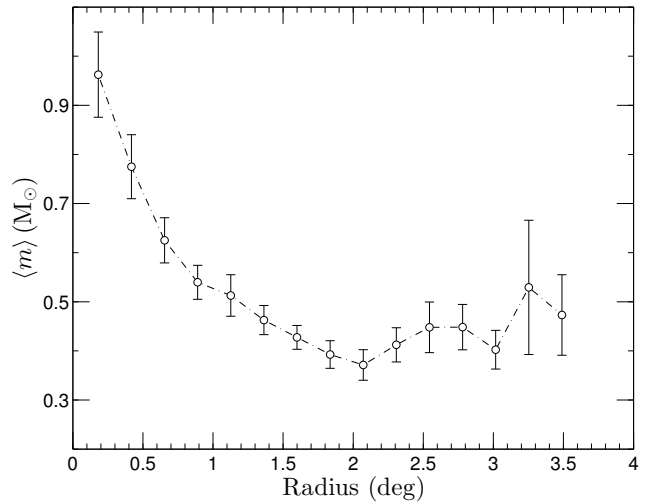
**Figure 6.** Surface density of all ($J \leq 15.5$, upper line), faint ($11 < J \leq 15.5$, middle line) and bright ($J \leq 11$, lower line) possible members in a 5-degree field around the centre of Praesepe. The dashed magenta line marks the tidal radius of Praesepe. To avoid confusion only error bars of the density of all stars are shown. The error bars are Poissonian.

4 RESULTS

4.1 Stellar mass function

As shown before, possible cluster members are mainly located within 3.5 degrees of the cluster centre so we restrict our study to stars within this radius when deriving the mass function. To obtain the mass function of the cluster members, we must statistically subtract the background level. This is done as follows:

- (i) In Fig. 6, we assume that all stars which reside between 4° and 5° are background stars.
- (ii) We derive the mass function of these background stars.
- (iii) We generate 84 random stars distributed according to the mass function derived in the previous step.
- (iv) Using these stars, we select possible members with similar mass and remove them from the list of possible members.

**Figure 7.** Normalized cumulative sums of stellar masses for bright (upper line), faint (lower line) and all (middle line) cluster members as functions of radius in a field of 3.5° from the new cluster centre. The dashed line intersects the total cumulative curve at half the maximum value corresponding to a half mass radius of 1.23° which is equivalent to 3.90 pc.**Figure 8.** The average mass of the possible cluster members as a function of radius from the centre of Praesepe. The average mass is roughly constant beyond 1.5°.

The mass function for the possible members after background subtraction is shown in Fig. 9. This figure shows that the mass function of Praesepe cannot be fitted by a single power-law distribution $dN/dm = \xi(m) \sim m^{-\alpha}$. As a result we assume that the mass function is described by a two-stage power-law distribution with a turnover at m_t , so that the mass function of stars with masses higher than m_t , hereafter high mass stars, is fitted by $\xi(m) \sim m^{-\alpha_{\text{high}}}$, whereas the mass function of those lower than m_t , hereafter low mass stars, is fitted by $\xi(m) \sim m^{-\alpha_{\text{low}}}$. The method

we use to derive m_t and the value of each α is based on a maximum-likelihood fitting combined with a Kolmogorov-Smirnov test to evaluate the goodness of the fit. This method was introduced by [Clauset et al. \(2009\)](#) for the case that the exponent of the power-law α is greater than unity and there exists a lower bound to the data. We re-derive the relations for both $\alpha > 1$ and $\alpha < 1$ and when the data is bounded on two sides. The case of two-sided bounds is important in our case, since stars more massive than $2.20 M_\odot$ have evolved off the main sequence while stars less massive than $0.15 M_\odot$ are too faint to be detected. The details of this method and the derivation of α values and their corresponding errors are presented in appendix A. This method provides much more accurate results compared to using a least-squares method on binned data ([Clauset et al. 2009](#)).

Using the method mentioned above, we find that a K-S test indicates with high confidence (5% significance level) that the turnover in the mass function is at $m_t = 0.65 M_\odot$ which is also visible in the figure. We also obtain $\alpha_{\text{low}} = 0.85 \pm 0.10$ and $\alpha_{\text{high}} = 2.88 \pm 0.22$ for low and high mass stars respectively. According to the K-S test our result for the overall mass function would also be consistent with a turnover at $0.5 M_\odot$ and in such a case the mass functions slopes would be $\alpha_{\text{low}} = 0.72 \pm 0.13$ and $\alpha_{\text{high}} = 2.51 \pm 0.15$ (close to $\alpha = 2.35$ found by [Salpeter 1955](#)).

Since the total mass of Praesepe is about $\sim 500 M_\odot$ and the 3D half-mass radius is $\sim 5.20 \text{ pc}$, the age of Praesepe is approximately ~ 5 times its relaxation time and one can assume that the stellar content of the cluster has thoroughly mixed in the entire cluster, meaning that the location of the turnover in the mass function should not change from one point to another. We therefore fix the location of the turnover and derive the mass function slopes inside and outside the half-mass radius. We find that the mass function slope of massive stars inside the half-mass radius ($\alpha = 2.32 \pm 0.24$) is less steep than the overall slope ($\alpha_{\text{high}} = 2.88 \pm 0.22$). However in the outer radial bin, the mass function of massive stars becomes steeper ($\alpha = 4.90 \pm 0.51$), and this is again indicating mass segregation in Praesepe.

To correct for the effect of unresolved binaries on the observed mass function, we did a series of a simulations which are discussed in Section 4.3.

4.2 Comparison to other works

Table 4 compares mass function slopes for Praesepe as obtained by various studies within the last 20 years. In this table only those studies whose mass range overlaps our studied mass range are listed.

We obtain $\alpha = 0.85 \pm 0.10$ for stars in the mass range $0.15 \leq m/M_\odot \leq 0.65$. Within the error bars, this value is in good agreement with [Baker et al. \(2010\)](#) and [Boudreault et al. \(2012\)](#), however it is steeper than the value found by [Adams et al. \(2002\)](#). This disagreement, as discussed by [Boudreault et al. \(2010\)](#), is most likely due to the fact that the membership criterion of [Adams et al. \(2002\)](#) is based on a threshold for the membership probability of only $p = 0.01$, which increases the likelihood of contamination by background stars. The value that we have found for the low-mass slope of the mass function is less steep than the values found by [Hambly et al. \(1995\)](#) ($\alpha = 1.5$), [Kraus &](#)

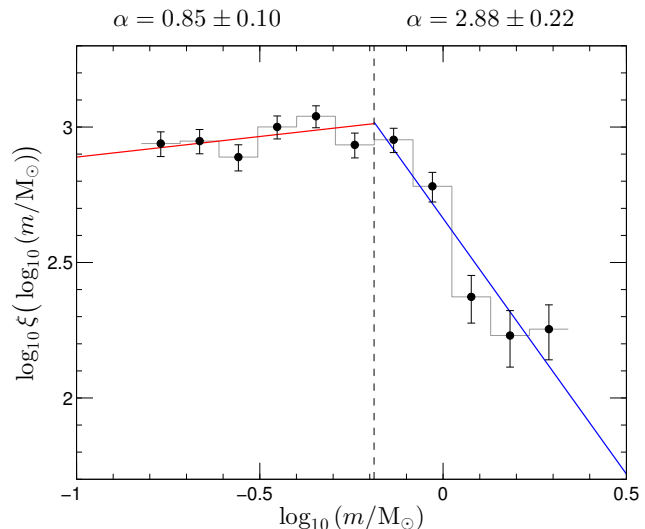


Figure 9. Mass function of stars in Praesepe corrected for background stars. Error bars of data points are Poissonian. Dashed line which corresponds to $m = 0.65 M_\odot$ shows the point at which the mass functions has a turnover. Red ($\alpha = 0.85 \pm 0.10$) and blue ($\alpha = 2.88 \pm 0.22$) lines show the best fit to the mass function of low-mass and high-mass stars respectively. While in this figure data is binned, the procedure we use to determine the α values does not work with binned data.

[Hillenbrand \(2007\)](#) ($\alpha = 1.4 \pm 0.2$) and [Boudreault et al. \(2010\)](#) ($\alpha = 1.8 \pm 0.1$). The discrepancy with [Boudreault et al. \(2010\)](#) is due to the fact that they identified the members of Praesepe only through photometry, while [Boudreault et al. \(2012\)](#) used proper motions combined with photometry, which led to the rejection of more background stars. [Boudreault et al. \(2012\)](#) found 1116 members for Praesepe among which 855 stars have $J \leq 15.5 \text{ mag}$ (our survey limit) and 552 of these stars ($\sim 65\%$) are recovered by our analysis.

Hence, three recent independent studies (our work, [Boudreault et al. 2012](#) and [Baker et al. 2010](#)) show a turnover at $\sim 0.5 \pm 0.1 M_\odot$ in the mass function and a slope of $\alpha \approx 0.8$ for the mass function before the turnover.

4.3 Binary fraction

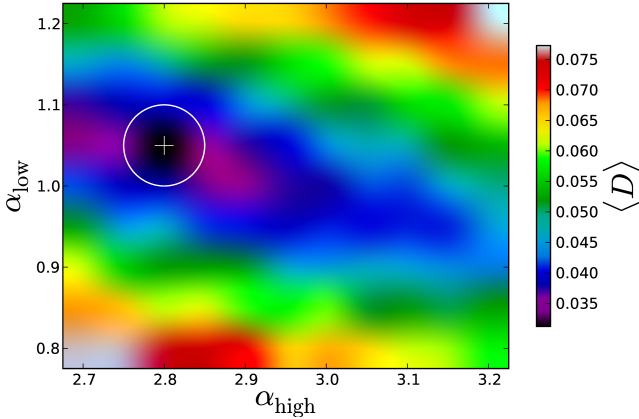
Figure 3 shows that there are a number of stars which reside above the main sequence of the isochrone (filled green triangles). This deviation is significantly outside the error bars for the photometry, so it suggests the presence of binary systems in the cluster. The CMD shows that there are also stars (depicted by open magenta squares in Fig. 3) that are more than 0.75 mag above the isochrone. Since these stars show a strong concentration towards the cluster centre as shown in Fig 5, they are most likely cluster members and are therefore either binaries or higher order multiple systems.²

There are 25 stars that deviate from the isochrone by more than 2.5σ , where σ refers to the mean error of the photometry. The corresponding binary fraction, which we

² By higher order multiples we mean triple, quadruple and more complex systems.

Table 4. A comparison of different profiles obtained for global mass function of Praesepe.

Reference	low-mass MF slope	high-mass MF slope
Our work (2013) corrected for binaries	$\alpha = 0.85 \pm 0.10$ $0.15 \leq M/M_{\odot} \leq 0.65$	$\alpha = 2.88 \pm 0.22$ $0.65 \leq M/M_{\odot} \leq 2.20$
	$\alpha = 1.05 \pm 0.05$	$\alpha = 2.80 \pm 0.05$
Boudeault et al. (2012)	$\alpha = 0.63 \pm 0.11^a$ $0.062 \leq M/M_{\odot} \leq 0.695$	– –
Boudeault et al. (2010)	$\alpha = 1.8 \pm 0.1$ $0.1 \leq M/M_{\odot} \leq 0.6$	– –
Baker et al. (2010)	$\alpha = 1.10 \pm 0.37$	–
	(Z band) $0.125 \leq M/M_{\odot} \leq 0.6$	–
	$\alpha = 1.07$	–
	(J band) $0.20 \leq M/M_{\odot} \leq 0.5$	–
Kraus & Hillenbrand (2007)	$\alpha = 1.09$	–
	(K band) $0.20 \leq M/M_{\odot} \leq 0.5$	–
	$\alpha = 1.4 \pm 0.2$ $0.12 \leq M/M_{\odot} \leq 1$	– –
Adams et al. (2002)	$\alpha = 0$ $0.1 \leq M/M_{\odot} \leq 0.4$	$\alpha = 1.6$ $0.4 \leq M/M_{\odot} \leq 1$
Hambly et al. (1995)	$\alpha = 1.5$ $0.1 \leq M/M_{\odot} \leq 0.5$	

Table 4. a) The value of $\alpha = 0.63 \pm 0.11$ is not reported in Boudeault et al. (2012). We derive this value using the original data given in Table 3 of the corresponding paper.**Figure 10.** The value of the KS statistic D between the outcome of the simulations (averaged over 50 different random seed numbers) and the observed mass function as a function of α_{low} and α_{high} for an assumed binary fraction of $f_{\text{bin}} = 35\%$. The white cross shows the location of the best match with observation. The white circle represents the lower limit of the errors in our simulation

define as the fraction of binary systems $f_{\text{bin}} = N_{\text{bin}}/(N_{\text{sing}} + N_{\text{bin}})$ is therefore $8.47\% \pm 1.55\%$ for $7.05 \leq J \leq 12.35$.

In order to recover the true binary fraction and the true mass function, we simulate the effect of binaries through a number of Monte Carlo simulations by constructing non-random pairs out of the single stars, assuming that the likelihood of each star to be chosen as a primary increases linearly with the logarithm of its mass, similar to what is seen in recent simulations of star formation (e.g. Bate 2009).

The procedure that we have adopted to derive the true binary fraction and mass function in our simulations is as follows:

- (i) Create a model cluster using a two-stage mass function with a mass function slope for low-mass stars α_{low} and a slope for high-mass stars α_{high} .
- (ii) Derive J and K_s magnitudes of the stars using the modified PADOVA isochrone.
- (iii) Select each primary component of a binary with a probability which is proportional to $\log_{10}(m_{\text{prim}}/m_{\text{min}})$. Here m_{prim} is the mass of each primary component and m_{min} is the minimum mass of all stars in the mass function.
- (iv) Select each secondary component (J_2, K_{s2}) based on a uniform (flat) distribution for mass ratios ($q = m_s/m_p$) between $0 < q < 1$.
- (v) Compute the total magnitude of the binary system:

$$J_{(\text{binary})} = -2.5 \log(10^{-0.4J_1} + 10^{-0.4J_2}) \quad (3)$$

$$K_{s(\text{binary})} = -2.5 \log(10^{-0.4K_{s1}} + 10^{-0.4K_{s2}}) \quad (4)$$

(vi) Add synthetic photometric errors to the magnitudes derived in the previous section. The synthetic photometric errors are generated in such way that they replicate the photometric errors of stars in PPMXL.

(vii) Determine the binary systems that deviate significantly from the isochrone and count them as observed binaries.

(viii) Compare the observed binary fraction in the simulation with the binary fraction from the simulation and the mass function of the single stars and non-detected binaries with the observed mass function.

(ix) Change the parameters of the initial mass function

and the assumed binary fraction until the best match in terms of the KS statistic D with the observed mass function and the observed binary fraction is found.

The range of parameters that we use in our simulations to generate the model clusters is:

- $\alpha_{\text{low}} \in [0.8 : 0.05 : 1.2]$
- $m_t = 0.65 M_{\odot}$
- $\alpha_{\text{high}} \in [2.7 : 0.05 : 3.2]$

In order to reduce statistical random errors we run our simulation for 50 different random seed numbers and then take an average over the KS statistic D and $f_{\text{bin}}(\text{observed})$ for each set of given parameters.

According to our simulations, an assumed binary fraction of $f_{\text{bin}} = 35\% \pm 5\%$ in the mass range $0.6 \leq m/M_{\odot} \leq 2.20$ ($7.05 \leq J \leq 12.35$) and an initial mass function with $\alpha_{\text{low}} = 1.05 \pm 0.05$ and $\alpha_{\text{high}} = 2.80 \pm 0.05$ yields the best agreement with the observed mass function and observed binary fraction. The fact that α_{low} which is obtained from simulations is steeper than than the observed (uncorrected) value is to be expected since many low-mass stars will be hidden in binaries with more massive companions.

Fig. 10 shows the value of KS statistic D as a function of α_{low} and α_{high} for $f_{\text{bin}} = 35\%$. The best match with the observation is obtained by minimizing the value of D and its location in the parameter space is shown by the white cross. As shown in the figure, one can see that the value of D strongly depends on α_{low} in contrast to α_{high} which does not change the value of D significantly.

Our simulations also reveal that due to photometric errors, a fraction of binaries scatter above the isochrone by more than $\Delta J = 0.75$ mag and are identified as fake multiples. According to our simulations, from 18 multiples detected in the CMD, 7 ± 2 can be explained by binaries this way. The rest are likely to be genuine multiples.

For comparison, [Bouvier et al. \(2001\)](#) found a binary fraction of $25.3 \pm 5.4\%$ for 149 G and K dwarfs observed in Praesepe using adaptive optics. According to our best fitting model, we find a binary fraction of $30 \pm 5\%$ for the same mass range which is roughly consistent with the results of [Bouvier et al. \(2001\)](#).

Finally, we estimate the total cluster mass. By summing up the masses of members obtained from our modified PADOVA isochrone and subtracting the contribution of contaminants we derive a total mass of $424 M_{\odot}$. By extending the global mass function profile to $0.08 M_{\odot}$ to compensate for missing low mass stars, this value increases to $448 M_{\odot}$. Assuming that there are no black holes or neutron stars left in the cluster, we also extend the global mass function profile to an initial mass of $8 M_{\odot}$ to calculate the contribution of white dwarfs to the total mass. We adopt the semi-empirical relation from [Kalirai et al. \(2008\)](#) which gives the final mass of white dwarfs as a function of the initial masses of the main-sequence progenitors. After this correction, the total mass is $465 M_{\odot}$. Due to binaries, which increase the mass by approximately a factor of 0.35, we derive a total mass of $\approx 630 M_{\odot}$ for Praesepe.

5 CONCLUSION

We have identified 893 possible members of the open cluster Praesepe using proper motions from the PPMXL catalogue and J and K photometry from the 2MASS and z photometry from SDSS in a field of 3.5° from the cluster centre.

We then calculated a new density centre for the cluster as defined by [von Hoerner \(1960, 1963\)](#) using the unbiased form of the local density estimator from [Casertano & Hut \(1985\)](#). Using this new cluster centre ($\alpha_{\text{centre}} = 8^h 39^m 37^s$, $\delta_{\text{centre}} = 19^{\circ} 35' 02''$) we derived the surface density profile, 2D half-number (4.25 pc) and half-mass radii (3.90 pc) for Praesepe. We found that Praesepe is strongly mass segregated.

We derived the global and radial mass functions of Praesepe. The global MF of Praesepe is a two-stage power law with $\alpha_{\text{low}} = 0.85 \pm 0.10$ and $\alpha_{\text{high}} = 2.88 \pm 0.22$ for low and high mass stars respectively and with a turnover at $0.65 M_{\odot}$. The value we have obtained for the slope of the mass function for low-mass stars ($\alpha_{\text{low}} = 0.85 \pm 0.10$) is consistent with [Baker et al. \(2010\)](#) and [Boudreault et al. \(2012\)](#). The presence and location of the turnover in the mass function at $m = 0.65 M_{\odot}$ is in agreement with [Boudreault et al. \(2012\)](#) who found that the mass function of Praesepe has a maximum at $0.6 M_{\odot}$. We also found that the high-mass slope of the radial mass functions increases from inner to outer radii, providing further evidence for mass segregation in Praesepe.

From an inspection of the CMD of Praesepe, we also identified 25 binaries and 18 multiple stars. Including unresolved binaries in the CMD, we did a series of simulations to recover the true binary fraction and the true initial mass function. According to our simulations the model which shows the best agreement with the observed mass function and binary fraction has an underlying mass function similar to the observed mass function but an overall binary fraction of $f_{\text{bin}} = 35\% \pm 5\%$.

Finally, we derive a mass of $424 M_{\odot}$ for Praesepe from the visible stars after subtracting the contribution of contaminants. By considering the contribution of low mass stars, white dwarfs and unresolved binaries this value increases to $\approx 630 M_{\odot}$.

ACKNOWLEDGMENTS

H.B. acknowledges support from the Australian Research Council through Future Fellowship grant FT0991052. The authors also would like to thank Wing Cheng and the anonymous referee for their useful comments.

REFERENCES

- Adams, J. D., Stauffer, J. R., Skrutskie, M. F., Monet, D. G., Portegies Zwart, S. F., Janes, K. A., Beichman C. A., 2002, AJ, 124, 1570
- Ahn, C. P., et al., 2012, ApJS, 203, 21
- Allard, F., Homeier, D., Freytag, B., 2011, ASPC, 448, 91
- An, D., Terndrup, D. M., Pinsonneault, M. H., Paulson, D. B., Hanson, R. B., Stauffer, J. R., 2007, ApJ, 655, 233
- Baker, D. E. A., Jameson, R. F., Casewell, S. L., Deacon, N., Lodieu, N., Hambly, N., 2010, MNRAS, 408, 2457
- Bate, M. R., 2009, MNRAS, 392, 590
- Boesgaard, A. M., Budge, K. G., 1988, ApJ, 332, 410

- Boesgaard, A. M., 1989, ApJ, 336, 798
 Boudreault, S., Bailer-Jones, C. A. L., Goldman, B., Henning, T., Caballero, J. A., 2010, A&A, 510, 27
 Boudreault, S., Lodieu, N., Deacon, N. R., Hambly, N. C., 2012, MNRAS, 426, 3419
 Bouvier, J., Duchene, G., Mermilliod, J.-C., Simon T., 2001, A&A, 375, 989
 Casertano S., Hut P., 1985, ApJ, 298, 80
 Chappelle, R. J., Pinfield, D. J., Steele, I. A., Dobbie, P. D., Magazzù, A., 2005, MNRAS, 361, 1323
 Clauset, A., Shalizi, C. R., Newman, M. E. J., 2009, SIAM Rev., 51(4), 661
 Fisher, R. A., 1922, Phil. Trans. R. Soc. Lond. A, 222, 309
 Fossati L., Bagnulo S., Landstreet J., Wade G., Kochukhov O., Monier R., Weiss W., Gebran M., 2008, A&A, 483, 891
 Friel, E. D., Boesgaard, A. M., 1992, ApJ, 387, 170
 Gaburov, E., Gieles, M., 2008, MNRAS, 391, 190
 Girardi, L., et al., 2010, ApJ, 724, 1030
 González-García, B. M., Zapatero Osorio, M. R., Béjar, V. J. S., Bihain, G., Barrado y Navascués, D., Caballero, J. A., Morales-Calderón, M., 2006, A&A, 460, 799
 Hambly, N. C., Steele, I. A., Hawkins, M. R. S., Jameson, R. F., 1995, MNRAS, 273, 505
 Hauschildt, P. H., Allard, F., Baron, E., 1999, AJ, 512, 377
 Jones, B. F., Cudworth, K., 1983, AJ, 88, 215
 Jones, B. F., Stauffer, J. R., 1991, AJ, 102, 1080
 Kalirai, J. S., Hansen, B. M. S., Kelson, D. D., Reitzel, D. B., Rich, R. M., Richer, H. B., 2008, AJ, 676, 594
 Klein-Wassink, W. J., 1927, Publ. Kapteyn Astron. Lab., 41, 1
 Kraus, A. L., Hillenbrand, L. A., 2007, AJ, 134, 2340
 Küpper, A. H. W., Kroupa, P., Baumgardt, H., Heggie, D. C., 2010, MNRAS, 407, 2241
 Lyngå, G., 1987, Catalogue of open cluster data, 5th edition, Centre de Données Stellaires, Strasbourg
 Madsen, S., Dravins, D., Lindegren, L., 2002, A&A, 381, 446
 Monet, D. G., et al., 2003, AJ, 125, 984
 Marigo, P., Girardi, L., Bressan, A., Groenewegen, M. A. T., Silva, L., Granato, G. L., 2008, A&A, 482, 883
 Pace, G., Pasquini, L. François, P. 2008, A&A, 489, 403
 Pinfield, D. J., Hodgkin, S. T., Jameson, R. F., Cossburn, M. R., von Hippel, T., 1997, MNRAS, 287, 180
 Röser, S., Demleitner, M., Schilbach, E., 2010, AJ 139, 2440
 Röser, S., Schillbach, E., Piskunov, A. E., Kharchenko, N.V., Scholz, R.-D., 2011, A&A, 531, 92
 Salpeter, E. E., 1955, ApJ 121, 161
 Skrutskie, M. F., et al., 2006, AJ, 131, 1163
 Taylor, B. J. 2006, AJ, 132, 2453
 van Leeuwen F., 2009, A&A, 497, 209
 von Hoerner S., 1960, Z. Astrophys., 50, 184
 von Hoerner S., 1963, Z. Astrophys., 57, 47
 Wang, W., Boudreault, S., Goldman, B., Henning, Th., Caballero, J. A., Bailer-Jones, C. A. L., 2011, ASPC, 448, 761
 York, D. G., et al., 2000, AJ, 120,1579

APPENDIX A: ALGORITHM FOR FINDING THE MASS FUNCTION SLOPE AND BREAK POINT

A1 Deriving α and its error $\sigma(\alpha)$

For a power law distribution with both lower and upper bounds (x_{\min}, x_{\max}) the probability density function is

$$p(x) = Cx^{-\alpha}$$

where C is the normalisation constant and $\alpha \neq 1$.

The likelihood of the data given the model with scaling parameter α is

$$p(x|\alpha) = \prod_{i=1}^n (1-\alpha) \frac{x_i^{-\alpha}}{x_{\max}^{1-\alpha} - x_{\min}^{1-\alpha}}$$

The logarithm \mathcal{L} of the likelihood is

$$\mathcal{L} = \ln p(x|\alpha) = \ln \prod_{i=1}^n (1-\alpha) \frac{x_i^{-\alpha}}{x_{\max}^{1-\alpha} - x_{\min}^{1-\alpha}}$$

The *maximum likelihood estimate* for α is obtained when

$$\frac{\partial \mathcal{L}}{\partial \alpha} = 0$$

Setting $X = \frac{x_{\max}}{x_{\min}}$, we obtain

$$\begin{aligned} \frac{\partial \mathcal{L}}{\partial \alpha} &= \frac{n}{\alpha - 1} - \sum_{i=1}^n \ln \frac{x_i}{x_{\min}} + n \frac{\ln X}{1 - X^{\alpha-1}} \\ \rightarrow \alpha &= 1 + n \left[\sum_{i=1}^n \ln \frac{x_i}{x_{\min}} - n \frac{\ln X}{1 - X^{\alpha-1}} \right]^{-1} \end{aligned} \quad (\text{A1})$$

Eq. (A1) is a general formula which holds for both $\alpha < 1$ and $\alpha > 1$. In general one needs to use numerical methods to calculate α from Eq. (A1) since there is no general analytic solution to this equation. However, if we assume that there is only a lower bound on data then for $\alpha > 1$ the last term of Eq. (A1) vanishes and there is an analytic solution as follows (also given in Clauset et al. 2009)

$$\alpha = 1 + n \left[\sum_{i=1}^n \ln \frac{x_i}{x_{\min}} \right]^{-1}$$

To estimate the error of α we need to calculate the variance of α as explained in Fisher (1922) which is

$$\sigma^2(\alpha) = - \left(\frac{\partial^2 \mathcal{L}}{\partial \alpha^2} \right)^{-1} \quad (\text{A2})$$

By substituting \mathcal{L} into Eq. (A2) one obtains

$$\sigma(\alpha) = \frac{1}{\sqrt{n}} \left((\alpha - 1)^{-2} - \ln^2 X \frac{X^{\alpha-1}}{(1 - X^{\alpha-1})^2} \right)^{-1/2} \quad (\text{A3})$$

Again if we assume that there is only a lower bound on data then for $\alpha > 1$, Eq. (A3) reduces to the following equation which is given in Clauset et al. (2009)

$$\rightarrow \sigma(\alpha) = \frac{|\alpha - 1|}{\sqrt{n}}$$

A2 Finding the mass function turnover (break point)

So far we have derived Eq. (A1) and Eq. (A3) to estimate α and its error $\sigma(\alpha)$. However, often mass functions of stellar clusters show a turnover. To find the mass function turnover we proceed as follows:

1. Decide on the mass range in which the turnover (m_t) lies. Let I_M denote the selected mass range.

2. Pick a mass (say m_x) from I_M .

3. Fit two power law functions to the data. One from m_{\min} to m_x and the other from m_x to m_{\max} ³. Calculate the corresponding α values using Eq. (A1).

4. Make two theoretical power law distributions using the calculated α values and combine these two theoretical distributions to obtain one overall distribution for the whole mass range.

5. Compare this distribution with the observed distribution using a Kolmogorov-Smirnov test and record the K-S statistic D .

6. Vary m_x in I_M until D obtains a minimum. The mass for which D becomes minimized is the turnover.

Following the procedure explained above, one can see that m_t , α and $\sigma(\alpha)$ are calculated all at once.

³ m_{\min} and m_{\max} correspond to the whole mass range and not to I_M defined in step 1.